J. Electrochem. Sci. Eng. **13(2)** (2023) 407-420; http://dx.doi.org/10.5599/jese.1369

Open Access : : ISSN 1847-9286
https://pub.iapchem.org/ojs/index.php/JESE

Review paper

High-velocity air fuel coatings for steel for erosion-resistant applications

Yasemin Yıldıran Avcu[1], Mert Guney[2,✉] and Egemen Avcu[1,✉]

[1]*Department of Mechanical Engineering, Natural and Applied Sciences, Kocaeli University, Kocaeli 41001, Turkey*

[2]*School of Engineering and Digital Sciences, Department of Civil and Environmental Engineering, The Environment & Resource Efficiency Cluster (EREC), Nazarbayev University, Nur-Sultan 010000, Kazakhstan*

Corresponding authors: ✉mert.guney@nu.edu.kz; ✉avcuegemen@gmail.com

Received: April 30, 2022; Accepted: July 1, 2022; Published: July 28, 2022

Abstract

High-velocity air fuel (HVAF) coating processes have advantages over conventional high-velocity oxygen fuel (HVOF) processes, resulting in coatings with superior properties. The present review first provides a concise overview of HVAF coatings, highlighting their advantages over HVOF coatings. Then, the fundamentals of solid particle, slurry, and cavitation erosion are briefly introduced. Finally, the performance of HVAF coatings for erosion-resistant applications is discussed in detail. The emerging research consistently reports HVAF-coatings having higher erosion resistance than HVOF-coatings, which is attributed to their elevated hardness and density and improved microstructural features that inhibit the surface damages caused by erosion. The dominant wear mechanisms are mainly functions of particle impact angle. For instance, the removal of the binder phase at high impact angles causes the accumulation of plastic strain on hard particles (e.g., WC particles) in the matrix, forming micro-cracks between the hard particles and the matrix, eventually decreasing the erosion resistance of HVAF coatings. The binder phase of HVAF-coatings significantly affects erosion resistance, primarily due to their inherent mechanical properties and bearing capacity of hard particles. Optimizing spraying parameters to tailor the microstructural characteristics of these coatings appears to be the key to enhancing their erosion resistance. The relationship between microstructural features and erosion mechanisms needs to be clarified to process coatings with tailored microstructural features for erosion-resistant applications.

Keywords

Thermal spraying; high velocity air fuel (HVAF); high velocity oxygen fuel (HVOF); slurry erosion; solid particle erosion; cavitation

Brief introduction to HVAF coatings

High-velocity air fuel (HVAF) is a relatively new thermal spray process compared to more established ones like high-velocity oxygen fuel (HVOF). HVAF has recently attracted interest for applications involving the deposition of wear-resistant alloys and cermet coatings [1]. Cermet-, iron-, and nickel-based coatings have primarily been deposited on substrates (the majority of which are steel) for solid particle erosion-, slurry erosion-, and cavitation erosion-resistant applications such as hydro turbines, circulating fluidized bed combustors, and boilers.

The HVAF process (Figure 1) involves several steps: first, a gaseous fuel (propane, propylene, or natural gas) and compressed air are mixed in a premixing chamber and then ignited at the front of a ceramic plate. Secondly, the reaction in the combustion chamber produces high-temperature and high-pressure gas, heating and accelerating the powder injected into the process *via* N_2 gas. Lastly, the gas flow is further accelerated to supersonic speeds through a divergent nozzle [2], depositing molten and semi-molten powder particles onto the substrate and providing a protective coating [3].

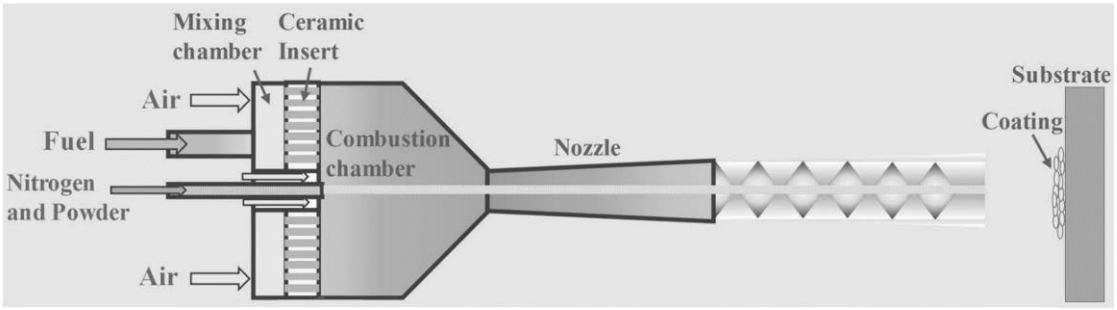

Figure 1. *Schematic presentation of the HVAF process. Reprinted with permission from reference [2]. Copyright (©) 2019 Springer Nature*

Numerous studies so far have reported the advantages of HVAF over HVOF, such as higher deposition rate and efficiency [1], higher jet velocity [4,5], and lower spray/flame temperature [4,5]. Using compressed air instead of O_2 helps to reduce flame and particle temperatures [6], assisting in maintaining raw material properties via inhibiting fine particle oxidation during spraying [4]. Furthermore, particles can reach higher velocities in HVAF compared to HVOF (up to 1,000 m/s), resulting in the deposition of very dense coatings [6,7]. Consequently, dense, highly cohesive coatings with low porosity, and superior wear performance can be deposited via HVAF [4,6,8]. Therefore, HVAF-coatings tend to exhibit higher mechanical properties (*i.e.*, fracture toughness, elasticity modulus, hardness, and compressive strength) than HVOF-coatings [5,9] due to the abovementioned advantages.

As HVAF-coatings have received increased attention in parallel to the development of thermal spray processes utilizing lower particle temperatures and higher particle velocities [10], there is an expanding effort to develop erosion-resistant HVAF-coatings, which comprises the subject of the present review. Here, the development of erosion-resistant HVAF-coatings in terms of their erosion properties is evaluated and discussed, while their microstructural and mechanical properties are briefly presented.

Brief introduction to erosion

Erosion could be defined as the progressive material removal from a target surface due to the repeated impact of solid particles carried by gaseous or liquid media [11,12]. It can be utilized to tailor surface properties (*e.g.*, grit and sandblasting [13]) or machine engineering materials (*e.g.*,

abrasive water jet cutting [14]) [15]. Solid particle and slurry erosion are also important industrial problems that cause wear, roughening, and degradation of engineering components, which may eventually lead to their premature failure in engineering applications [15,16].

Various engineering applications, including aerospace (*e.g.*, steam and jet turbine components, helicopter rotor blades) and power plant applications (*e.g.*, fluidized bed combustion systems, pipelines and valves carrying particulate matter in mining and oil transportation [17]) are typically vulnerable to erosion [15,16]. Any erosion-related failure of engineering components in these applications may result in safety concerns, financial overburden due to expensive repairing costs and production outages, and possible harmful environmental effects such as oil leakage [17]. Therefore, the erosion behavior of materials used in these applications must be clearly understood to improve their longevity and prevent erosion-related failures. Recently, there has been an interest in understanding the erosion behavior of newly developed erosion-resistant coatings, which is usually a complex phenomenon. The present section briefly explains the type of erosion that occurs on HVAF-coatings. It also describes the fundamentals of erosion along with the methods that are used to investigate the erosion behavior of materials.

The literature generally classifies erosion under four different groups/systems: (1) solid particle erosion, (2) slurry erosion, (3) cavitation erosion, and (4) water droplet erosion (Figure 2). In solid particle erosion, wear occurs due to the repeated impact of solid particles carried and accelerated by pressurized air/gas, whereas in slurry erosion, particles are carried and accelerated by a liquid medium. Slurry erosion can be carried out *via* two distinct methods/devices: jet type and rotating type equipment. In cavitation erosion, wear occurs due to the repeated impact of cavitation bubbles under high-turbulent fluid flow [18]. Finally, water droplet erosion (not covered in the present review) occurs via progressive material removal from a surface due to the repeated impact of droplets [5].

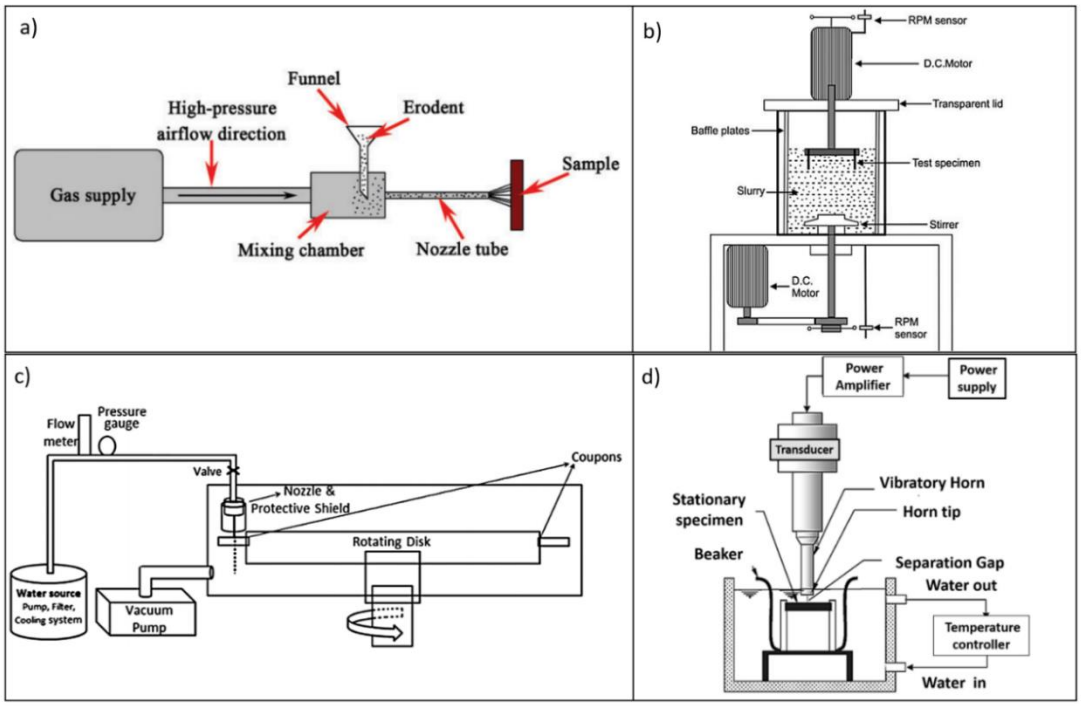

Figure 2. *Schematics of different erosion test rigs. a) Solid particle erosion. Reprinted with permission from reference [19], © 2015 SAGE Publications. b) Slurry erosion (rotating type). Reprinted with permission from reference [20], © 2015 Elsevier. c) Water droplet erosion. Reprinted with permission from reference [21], © 2015 Elsevier. d) Cavitation erosion. Reprinted with permission from reference [18], © 2016 Springer Nature*

The wear mechanisms causing erosion damage differ as a function of numerous parameters, such as particle properties, target material, and impingement conditions. After performing the erosion tests described above, the erosion rates, surface topography, morphology, hardness, and surface and cross-sectional microstructures of eroded samples could be examined via scanning electron microscopy, non-contact profilometry, and microhardness testing. The emerging literature on the solid particle, slurry, and cavitation erosion of HVAF-coatings is discussed below.

HVAF coatings for erosion-resistant applications

HVAF coatings against solid particle erosion

Table 1 summarizes studies on understanding solid particle erosion behavior of HVAF-coatings along with utilized HVAF and solid particle erosion parameters. Matthews *et al*. [22] reported the first study revealing the solid particle erosion behavior of HVAF- and HVOF-sprayed carbide-based coatings (Cr_3C_2–25NiCr) using an air jet erosion rig and SEM (Table 1). HVAF-coatings exhibited better erosion resistance than HVOF-coatings, which was attributed to the variation of erosion mechanisms depending on the coatings microstructure. Similarly, HVAF-sprayed FeCrNiMoBSiC amorphous coatings showed higher erosion resistance than HVOF-sprayed, which was attributed to the higher hardness of HVAF-coatings compared to HVOF (956 ± 56 HV0.1 *vs.* 821 ± 72 HV0.1) [23]. However, Baiamonte *et al*. [24] reported similar erosion behavior of HVAF-sprayed carbide-based cermet coatings and HVOF-sprayed coatings in terms of erosion rates, volume loss, and observed erosion mechanisms as a function of impingement angle.

Table 1. *HVAF coatings developed against solid particle erosion*

Reference	Coating	HVAF parameters	Solid particle erosion parameters
[22]	Cr_3C_2-25NiCr	Substrate: mild steel Fuel: kerosene Fuel consumption: 23 L / h Oxidant: O_2 Feeding gas: nitrogen Powder feed rate: 35 g / min	Air jet erosion rig (ASTM G76) Erodent: alumina Erodent diameter: 20 µm Impact angle: 90° Erodent velocity: 150 m / s Standoff distance: 25 mm
[19]	WC-10Co-4Cr	Substrate: 0Cr13Ni5Mo Fuel: propane Combustion gas: O_2 Feeding gas: N_2 Powder feed rate: 50-150 g / min Coating thickness: 180-450 µm	Air jet erosion rig (ASTM G76-83) Erodent: alumina Erodent diameter: 48-58 µm Erodent mass feed rate: 5 g / min Impact angle: 15°, 45°, 75°, 90° Erodent velocity: 90 m / s Standoff distance: 10 mm
[25]	WC-10Co-4Cr	Substrate: stainless steel Fuel: propane Combustion gas: O_2 Feeding gas: N_2 Powder feed rate: 50-150 g/min Coating thickness: 180-450 µm	Air jet erosion rig (ASTM G76-83) Erodent: alumina Erodent diameter: 48-58 µm Erodent mass feed rate: 5 g / min Impact angle: 15°, 90° Erodent velocity: 30 m / s Standoff distance: 10 mm
[26]	86WC-10Cr-4Co	Substrate: CA6NM hydro turbine steel Standoff distance: 300 mm Feed rate: 200 g / min Deposition rate: 20 µm / pass Coating thickness: 341 µm	Air jet erosion rig (ASTM G76) Erodent: alumina Average size: 50 µm Impact angle: 30˚, 60˚, 90˚ Time: 10 min Erodent discharge: 2 g / min Erodent velocity: 35, 70 m / s Nozzle diameter: 1.5 mm Standoff distance: 10 mm

Reference	Coating	HVAF parameters	Solid particle erosion parameters
[23]	FeCrNiMoBSiC	Substrate: low alloyed Mo steel Fuel: propane Combustion gas: O_2 Feeding gas: N_2 Powder feed rate: 100 g / min Coating thickness: 300 µm	Air jet erosion rig (ASTM G76-07) Air pressure: 10 kPa Erodent: alumina Erodent diameter: 50 µm Erodent feed rate: 5 g / min Impact angle: 90˚ Erodent velocity: 40 m / s Standoff distance: 10 mm
[24]	Cr_3C_2-10NiCr Cr_3C_2-FeNi Cr_3C_2-WC-MA	Substrate: carbon steel, Nozzle diameter:15 mm, Air: 690 kPa Fuel: 690 kPa Powder feed rate: 100-120 g / min Coating thickness: 180-200 µm	Air jet erosion rig (ASTM G76) Erodent: alumina (D_{50}=50) Angle: 30°, 90° Time: 10 min Erodent feed rate: 5 g / min Erodent velocity: 30 m / s
[6]	WC-NiMoCrFeCo WC-FeNiCrMoCu WC-FeCrAl	Substrate: high-strength low-alloy steel Fuel: propane Feeding gas: nitrogen Powder feed rate: 200 g / min Coating thickness: 250 µm	Air jet erosion rig (ASTM G76) Erodent: alumina Erodent diameter: 50 µm Erodent feed rate: 2 g / min Impact angle: 90˚ Erodent velocity: 30-70 m / s Standoff distance: 10 mm

Li *et al.* [19] showed that erosion and deformation mechanisms (*e.g.* crack formation and propagation) of HVAF-sprayed WC-Co-Cr coatings were strongly related to the coating microstructure. The variation of particle impingement angle affected the dominant erosion mechanism: micro-cutting was active at low impingement angles (<30°), whereas spallation was dominant at higher angles (<75°). Lian *et al.* [25] presented similar results where the erosion mechanisms were highly dependent on the microstructure of HVAF-sprayed WC-Co-Cr coatings. Briefly, coatings with a denser and more uniform microstructure have exhibited higher erosion resistance. The removal of Co-Cr binder was dominant at lower impingement angles, whereas severe plastic deformation and fracturing occurred at higher angles, causing an increased erosion rate at 90° impingement angle compared to those at lower angles.

Hamilton *et al.* [26] schematically presented the material removal mechanisms at 90° impingement angle and showed an increased erosion rate at normal impact angles. Briefly, the removal of the binder phase at high impact angles causes the accumulation of plastic strain on WC particles in the matrix, resulting in the formation of micro-cracks between the WC particles and the matrix (Figure 3). Then, loose WC particles could easily be removed from the surface due to erodent particle impact.

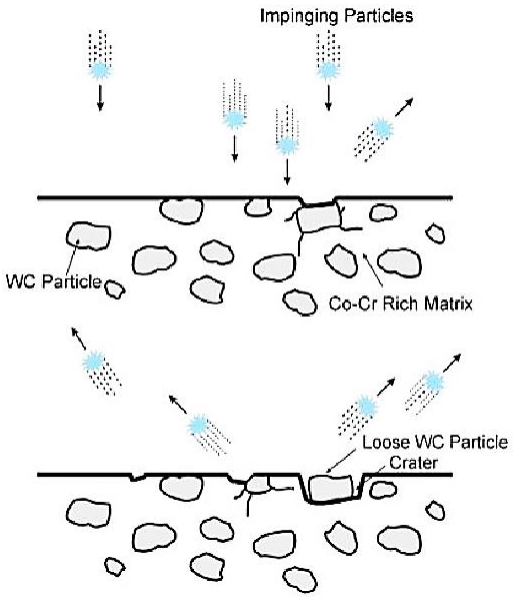

Figure 3. *Schematic of material removal mechanisms at high impingement angles during solid particle erosion of HVAF-coatings. Reprinted with permission from reference [26] © 2017 World Scientific Publishing*

Torkashvand *et al.* [6] also studied the solid particle erosion behavior of HVAF-sprayed WC-based coatings with binders with no or limited content of Co. The eroded coatings (WC-NiMoCrFeCo, WC-FeNiCrMoCu, and WC-FeCrAl) exhibited comparable wear mechanisms; indentation, ploughing, and shoveling wear mechanisms are depicted in Figure 4(a) and subsurface cracks and chipping mechanisms are shown in Figure 4(b). Due to a combination of deep ductile grooving (cutting, ploughing, and indentation (Figure 4(d)) and subsurface brittle fracture, severe erosive wear occurred for the WC-NiMoCrFeCo coating compared to other coatings. To sum up, the replacement of Co binders with environment-friendly binders appears promising for preserving the erosion resistance of HVAF-coatings [6] (Figure 4(c)).

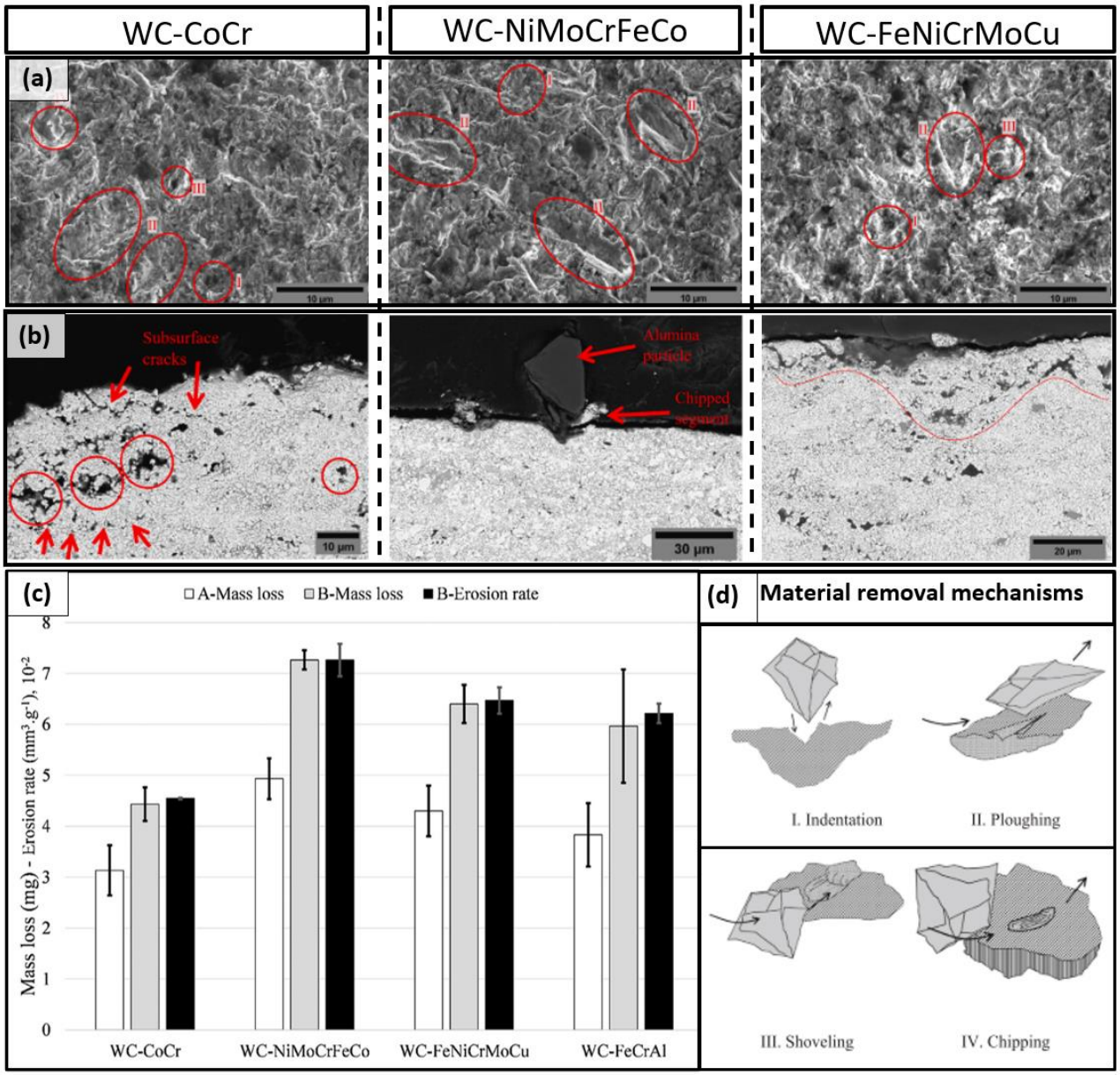

Figure 4. *a) Surface morphology after erosion, b) cross-sectional morphology after erosion tests, c) mass loss and erosion rate of the coatings, d) material removal mechanisms. Reprinted with permission from reference [6], © 2022 Elsevier*

HVAF coatings against slurry erosion

Table 2 summarizes studies on understanding the slurry erosion behavior of HVAF-coatings along with utilized HVAF and slurry erosion parameters. Liu *et al.* [27] examined the effect of nano-WC-

12Co powder reinforcement in HVAF-sprayed WC-10Co-4Cr coatings and showed that powder reinforcement improved erosion resistance and hardness compared to that of unreinforced coating, suggesting the use of nano-WC-12Co powder rather than micro-sized WC particles. Wang *et al*. [28] deposited WC-10Co-4Cr coatings on low-carbon steel substrates using HVOF and HVAF and then examined their slurry erosion resistance, aiming to develop erosion-resistant coatings for hydro-turbine components. It was shown that HVAF-coatings exhibited better erosion performance along with higher hardness and fracture toughness. Micro-cutting and micro-ploughing were the primary erosion mechanisms at low impingement angles, whereas micro-cutting and micro-chiseling were active at high impingement angles, causing the removal of Co-Cr binder and pulling of WC particles within the microstructure. Besides, erodent particle size also affects the dominant erosion mechanisms. Figure 5 schematically depicts the active erosion mechanisms as a function of erodent size.

Table 2. *HVAF coatings developed against slurry erosion*

Reference	Coating	HVAF parameters	Slurry erosion parameters
[27]	Nano-WC-12Co powder addition in WC-10Co-4Cr	Substrate: AISI 304 stainless steel Fuel gas: propane Carrier gas: nitrogen Standoff distance: 150 mm Powder feed rate: 60 g / min Coating thickness: 400 µm	Jet-type slurry erosion rig (ASTM G-73) Erodent: quartz Erodent size: -400 to +650 µm Standoff distance: 35 mm Erodent concentration: 300 g 10 L water Velocity: 46 m / s Slurry flow: 468 L / min Impact angle: 30°
[29]	WC-12Co, CrC-25NiCr	Substrate: stainless steel matrix 0Cr13Ni5Mo Coating thickness: 350-400 µm	Rotating type slurry erosion rig (silt erosion) Circular velocity: 15.5 m / s Silt concentration: 14 kg / L (ds_{50}=38 µm)
[28]	WC-10Co-4Cr	Substrate: low carbon steel Fuel gas: propane Standoff distance: 150 mm Powder feed rate: 80 g / min Coating thickness: 300 µm	Jet-type slurry erosion rig (custom-made) Erodent: SiO_2 Erodent size: 40-70 µm Concentration: 1:10 (sand/water) Standoff distance: 25 mm Feed rate: 150 g / min Impact angle: 30°, 90° Pressure: 0.2 MPa Duration: 720 min
[30]	FeCrMoMnWBCSi	Substrate: 316L SS Fuel pressure: 70 psi Air pressure: 82 psi Standoff distance: 180 mm Powder feed rate: 3 g / min Coating thickness: 250 µm	Jet-type erosion testing rig Erodent: silica Erodent size: 75-150 µm Concentration: water +2 wt.% silica Jet velocity: 20 m / s Nozzle diameter: 3 mm Standoff distance: 5 mm
[31]	WC-10Co-4Cr	Substrate: SS410 Fuel gas: propane 83.8 PSIG Standoff distance: 7 in Spray particle velocity: 1010, 960, 895 m / s Deposit thickness per pass: 28 µm	Jet-type erosion testing rig Impact angle: 15˚, 30˚, 45˚, 60˚, 90˚ Jet velocity: 20, 27, 36 m / s Slurry concentration: 2 wt.%
[32]	WC-10Co-4Cr Cr_3C_2-25NiCr	Substrate: low carbon steel	Rotating type slurry erosion rig: (1) water+33 wt.% 0.1-0.6 mm quarts (2) water+33 wt.% 2-3 mm quarts Time: 4×20 min Erodent velocity: 16 m/s Centrifugal erosion tester Erodent: 0.1-0.6 mm quartz Erodent velocity: 80 m / s

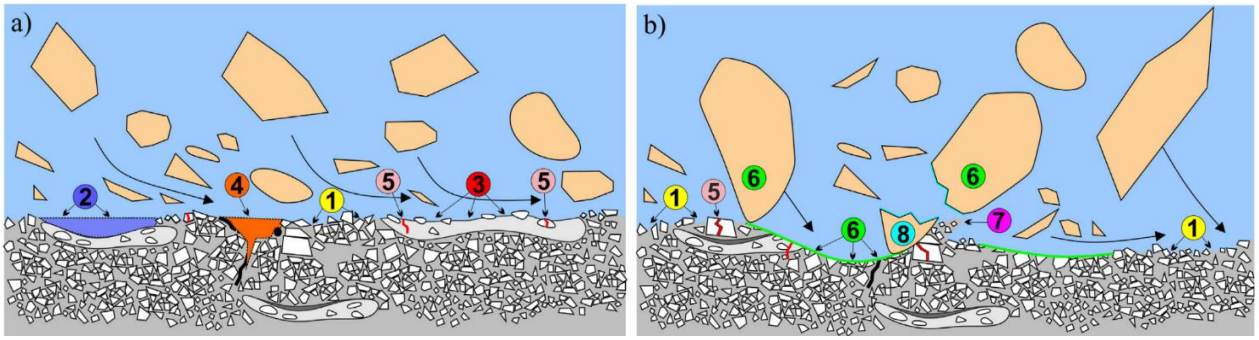

Figure 5. *Slurry erosion mechanism of carbide coatings as a function of erodent particle size a) fine quartz particles (0.1–0.6 mm) and b) coarse quartz particles (2–3mm): 1) removal of the soft metal matrix via selective erosion, 2) removal of weak coating area near-surface, 3) removal of the coating with low carbide content via selective erosion, 4) wear of weak splat interface, 5) micro-ploughing of coating by large particle, 6) lip formation due to plastic deformation, 7) fractured quartz fragment embedment and 8) carbide cracking. Reprinted with permission from reference [33], © 2019 Elsevier*

Kumar *et al.* [31] presented similar results, where the erosion rate of HVAF-sprayed WC-CoCr was 2.26 times higher than HVOF-coatings due to improved hardness, adhesion, and density of the HVAF-coatings. The erosion mechanisms were micro-cutting and micro-ploughing at low impingement angles and brittle cracking at high angles, in line with the results of Wang *et al*. [28]. Similar findings were reported in another study [30], where HVAF-sprayed FeCrMoMnWBCSi amorphous metallic coatings exhibited better erosion resistance than HVOF-coatings, which is attributed to superior microstructural and mechanical features of HVAF-coatings.

Matikainen *et al*. [33] compared the slurry erosion behavior of HVAF- and HVOF-sprayed WC-10Co4Cr and Cr_3C_2-25NiCr coatings and showed that HVAF was capable of producing slurry erosion-resistant coatings (Figure 6(a)). All surfaces in Figure 6 exhibited significant ploughing of material because of the repeated impacts of quartz particles. Figures 6(b) and 6(c) depict fine primary WC particles bulging from the surface along with some embedded quartz fragments indicated by white arrows (1). A lower microhardness revealed more distinct ploughing marks and localized material extrusion marked by green arrows (2). In Figures 6(c) and 6(d), the majority of the wear was caused by the ploughing of the material by large quartz particles, which resulted in the formation of a lip of extruded material (2). The higher kinetic energy of the quartz particles caused an increase in the number of surface fragments (1) [33].

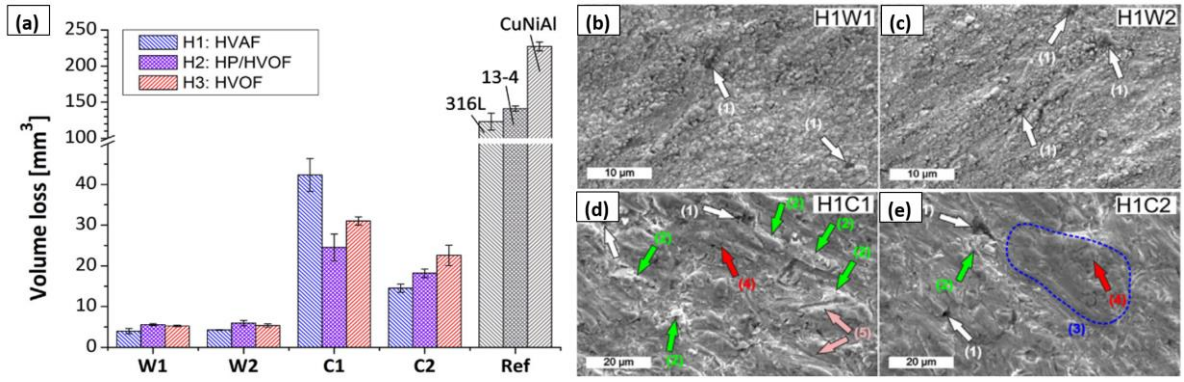

Figure 6. *a) Volume losses of coatings after slurry erosion, and worn surface of; b) WC-10Co4Cr (porous), c) WC-10Co4Cr (dense), d) Cr3C2-25NiCr (porous), e) Cr3C2-25NiCr (dense). Numbers indicate embedded quartz fragments (1), lip formation (2), carbide-rich clusters (3), carbide cracking (4) and coating cracking (5). Reprinted with permission from reference [33], © 2019 Elsevier*

HVAF coatings against cavitation erosion

Table 3 summarizes studies on understanding cavitation erosion behavior of HVAF-coatings along with utilized HVAF and cavitation erosion parameters. The cavitation erosion resistance of HVAF-sprayed 86WC-10Co4Cr [18], WC-10Co4Cr, WC-CoCr [10], Cr3C2-25NiCr [34], FeCrMnSiNi, FeCrMnSiB [35], Cr3C2–50NiCrMoNb, Cr3C2–25NiCr, and Cr3C2–37WC–18NiCoCr [36] coatings were superior to HVOF-coatings due to their lower porosity, higher hardness, higher toughness [18], and lower oxides content [35].

***Table 3**. HVAF coatings against cavitation erosion*

Reference	Coating	HVAF parameters	Cavitation erosion parameters
[18]	86WC-10Cr-4Co	Substrate: SS410 Air: 90.3 PSIG Propane: 83.8 PSIG Standoff distance: 7 in Spray particle velocity: 1010, 960, 895 m / s Deposit thickness per pass: 28 µm	Commercial ultrasonic processor Frequency: 20 kHz Solution: tap water
[34]	WC-10Co-4Cr Cr_3C_2-25NiCr	Substrate: S235 structural steel Fuel gas: propane Standoff distance: 300 mm Powder feed rate: 200 g / min (WC-10Co4Cr) Powder feed rate: 150 g / min (Cr3C2-25NiCr) Coating thickness: 300 µm	The alternative in-direct test method (ASTM G32-16) Frequency: 20 kHz Duration: 12 h
[33]	WC-10Co-4Cr Cr_3C_2-25NiCr	Substrate: S235 steel	The alternative in-direct test method (ASTM G32-16) Frequency: 20 kHz Solution: de-ionized water Duration: 8 h for coatings, 12 h for reference materials
[35]	FeCrMnSiNi FeCrMnSiB	Substrate: AISI/SAE 1020 Fuel gas: propane Standoff distance: 300 mm Powder feed rate: 90 g / min	The vibratory ultrasonic cavitation equipment in-direct test method (ASTM G32-16) Frequency: 20 kHz Solution: distilled water
[36]	Cr_3C_2–25NiCr Cr_3C_2-37WC-18NiCoCr Cr_3C_2-50NiCrMoNb	Substrate: S235 steel Fuel gas: propane Standoff distance: 300 mm Powder feed rate: 130-200 g / min Coating thickness: 300 µm	The alternative in-direct test method (ASTM G32-16) Frequency: 20 kHz Solution: de-ionized water Duration: 6 h
[37]	NiCrMoNb NiCrBSi	Substrate: steel Coating thickness: 350-400 µm	Ultrasonic vibration method Frequency: 20 kHz Solution: Tap water (12 V) Duration: 330 min
[10]	WC-10Co-4Cr	Substrate: S355 steel Fuel gas: propane Standoff distance: 250 mm Powder feed rate: 95 g / min	The vibratory ultrasonic cavitation equipment in-direct test method (ASTM G32-16) Frequency: 20 kHz Duration: 6 h
[9]	WC-10Co-4Cr WC-20CrC-7Ni	Substrate: AISI 1040 steel Fuel gas: propane Carrier gas: nitrogen Standoff distance: 180 mm Powder feed rate: 200 g / min Coating thickness per pass: 40 µm	Ultrasonic vibration method Frequency: 20 kHz Solution: tap water (pH 7.5, 8.5 V) Duration: 330 min
[7]	WC10Co4Cr WC20CrC7Ni	Substrate: structural steel Coating thickness: 400 µm	Ultrasonic vibration method Frequency: 20 kHz Time: 330 min Solution: tap water (pH 7.5, 8.5 V) Duration: 330 min

HVAF-sprayed NiCrMoNb coatings also exhibited promising cavitation resistance due to superior microstructural and mechanical features [37]. Varis *et al.* [10] proposed that high compressive stresses of HVAF-coatings inhibit the fatigue crack formation and propagation along the microstructure consisting of lamellae interfaces, thus improving the cavitation resistance of the coating. According to Korobov *et al*. [9], the fine structure of WC-CrC-Ni coating increases the specific surface area of carbide particles and, consequently, the required crack propagation energy.

In turn, this improves their resistance to chipping and consequently, to cavitation compared to the coarser WC-CoCr coating (Figure 7). In the case of the WC-CrC-Ni coating, the hardening of the matrix caused by the dissolution of Cr is accompanied by an increase in the matrix's plasticity, which prevents carbides from detaching from the matrix [9].

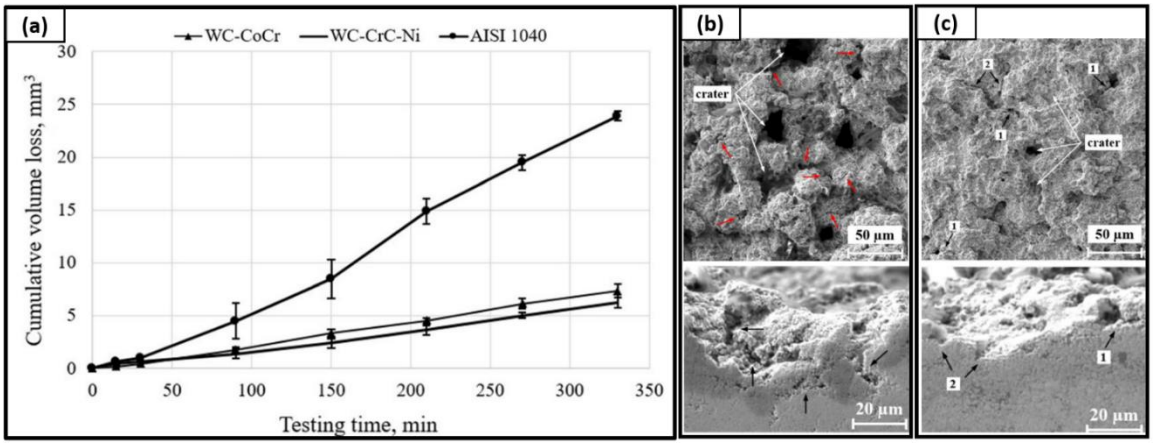

Figure 7. *a) Volume loss during cavitation test, SEM images of worn surfaces and subsurfaces of coatings; b) WC-CoCr, c) WC-CrC-Ni. Reprinted with permission from reference [9], © 2021 Springer Nature*

Kumar *et al*. [18] reported that spraying parameters (*e.g*., particle velocity) affected the mechanical properties of HVAF-sprayed tungsten carbide coatings (*e.g*., fracture toughness), influencing the resultant cavitation resistance. The coating microstructure (*i.e*., carbide content) was shown to affect the toughness and cavitation resistance [36]. The microstructural features of HVAF-coatings (*e.g*., pores and oxides) were the other key parameters affecting the cavitation resistance [35]. Commonly, the formation of deep and wide craters has been demonstrated on the surfaces of cavitation-eroded HVAF-coatings [7]. Furthermore, the repeated impact of cavitation bubbles has caused the formation of fatigue micro-cracks and severe plastic deformation within the microstructure. This leads to the removal of material from the surface [33]. Removal of material occurs through crack propagation due to the continuous implosion of cavitation bubbles [33].

Summary of HVAF coatings for erosion-resistant applications

So far, WCCoCr-, Cr_3C_2-, NiCr-, and FeCr-based coatings have been deposited on steel substrates for solid particle erosion-, slurry erosion-, and cavitation erosion-resistant applications. Table 4 provides a comparison of erosion-resistant HVAF coatings by listing their thickness, composition, and hardness, as well as active wear mechanisms and final remarks.

Table 4. *Erosion resistant HVAF coatings: a summary of compositions, hardness, thickness, wear mechanisms, and final remarks*

Coating	Coating composition	Coating properties	Erosion tests	Wear mechanisms	Final remarks
WCCoCr-based	WC-10Co-4Cr [7,9,10,18, 19,28,25,31-34] 86WC-10Cr-4Co [18,26] WC-NiMoCrFeCo [6] WC-FeNiCrMoCu [6] WC-12Co [29] WC-20CrC-7Ni [7,9]	Thickness: 180-450 µm Hardness: - WC-10Co-4Cr (850±90 - 1170±18 $HV_{0.5}$) - 86WC-10Cr-4Co (1290±30 - 1473±40 $HV_{0.3}$) - WC-NiMoCrFeCo & WC-FeNiCrMoCu - (1100 - 1300 $HV_{0.3}$) - WC-12Co (1160 HV) - WC-20CrC-7Ni (950±60 - 1160±90 $HV_{0.5}$)	• Solid particle erosion • Slurry erosion • Cavitation erosion	Severe plastic deformation, indentation, ploughing, shoveling, subsurface cracks and chipping mechanisms, and brittle fracture.	• HVAF coatings are harder, tougher, and more cavitation-resistant than HVOF coatings. • Porosity and hardness affect cavitation resistance. • - HVAF-coatings binder phase affects erosion resistance.

Coating	Coating composition	Coating properties	Erosion tests	Wear mechanisms	Final remarks
Cr_3C_2-based	Cr_3C_2-25NiCr [22,32-34,36] Cr_3C_2-10NiCr [24] Cr_3C_2-FeNi [24] Cr_3C_2-50NiCrMoNb [36] Cr_3C_2-37WC-18NiCoCr [36] Cr_3C_2-WC-MA [24]	Thickness: 180-300 µm Hardness: - Cr_3C_2-25NiCr (920±51-1002±69 $HV_{0.3}$) - Cr_3C_2-10NiCr (1080 $HV_{0.1}$) - Cr_3C_2-FeNi (965 $HV_{0.1}$) - Cr_3C_2-50NiCrMoNb (885±58 $HV_{0.3}$) - Cr_3C_2-37WC-18NiCoCr (1104±118 $HV_{0.3}$) - Cr_3C_2-WC-MA (1261 $HV_{0.1}$)	• Solid particle erosion • Slurry erosion • Cavitation erosion	Cutting and ploughing are the main wear mechanisms in solid particle erosion. Cavitation erosion causes coating fatigue wear, plastic deformation, and cracks.	• Due to their lower porosity, higher hardness, and higher toughness, HVAF coatings resist cavitation better than HVOF coatings. • HVAF produced slurry-resistant coatings. • Denser HVAF coatings resist slurry erosion better.
NiCr-based	NiCrMoNb [37] NiCrBSi [37]	Thickness: 350-400 µm Hardness: - NiCrMoNb (640±60 $HV_{0,05}$) - NiCrBSi (910±80 $HV_{0,05}$)	• Cavitation erosion	Not reported.	• NiCrMoNb coatings show higher cavitation resistance than NiCrBSi coatings.
FeCr-based	FeCrNiMoBSiC [23] FeCrMoMnWBCSi [30] FeCrMnSiNi [35] FeCrMnSiB [35]	Thickness: 250-300 µm Hardness: - FeCrNiMoBSiC (956±56 $HV_{0.1}$) - FeCrMoMnWBCSi (1433 $HV_{0.1}$) - FeCrMnSiB (557±40 $HV_{0.3}$) - FeCrMnSiNi (487±26 $HV_{0.3}$)	• Solid particle erosion • Slurry erosion • Cavitation erosion	Electrochemical and active corrosion mechanisms.	• High hardness and compactness of HVAF coatings improve erosion–corrosion resistance. • Lower porosity and oxide content in HVAF-coatings improve cavitation and corrosion resistance.

The following section provides key findings from the emerging literature on the development of erosion-resistant high velocity-air fuel (HVAF) coatings.

Conclusions

The present review critically reviews the emerging literature on the development of erosion-resistant high velocity-air fuel (HVAF) coatings. The performance of HVAF-coatings against solid particle erosion, slurry erosion, and cavitation erosion as a function of microstructural features, compositions, and mechanical properties is discussed. The dominant erosive wear mechanisms causing degradation of these coatings are addressed by providing eroded surface morphologies of the coatings subjected to different erosive wear conditions.

- So far, numerous cermet-, iron-, and nickel-based HVAF-sprayed coatings have been successfully deposited on steel substrates. These are promising for numerous engineering applications, including hydro turbines, circulating fluidized bed combustors, and boiler applications, due to their high solid particle, slurry, and/or cavitation erosion resistance.
- Due to enhanced microstructural and mechanical features (*i.e.,* dense microstructure and high hardness), the erosion resistance of HVAF-coatings is superior to that of HVOF-coatings. Optimizing spraying parameters to tailor the microstructural characteristics of these coatings appears to be the key to enhancing their erosion resistance.
- Clarifying the dominant erosion mechanisms under various erosion conditions is crucial for understanding how these recently developed coatings degrade over time. The binder phase of HVAF-coatings has been shown to significantly affect erosion resistance, primarily due to its inherent mechanical properties and bearing capacity of the hard particles (*e.g*., WC particles).
- To further improve the erosion resistance of HVAF coatings, the dominant erosion mechanisms and their progression through the coating's microstructure are the primary phenomena that

need to be revealed. These dominant wear mechanisms are mainly altered as a function of particle impact angle, where high impact angles cause more severe damage due to matrix micro-cracking, resulting in matrix and removal of hard particles from the microstructure.

- The relationship between microstructural features and erosion mechanisms has yet to be clarified to process coatings with tailored microstructural features for erosion-resistant applications. More widespread implementation of advanced microstructural and mechanical characterization methods (*e.g.,* FEG-SEM, nanoindentation) is required to understand the microstructural features of these coatings and their effects on the mechanical and erosion behavior. In addition, optimizing spraying parameters (*e.g.*, velocity) seems key to processing HVAF-coatings with high quality, on which the literature is limited. For field applications, parameter optimization studies involving "Design of Experiments (DoE)" are required that use robust design approaches (*e.g.*, Taguchi) to meet final product quality.

References

[1] P. S. Babu, Y. Madhavi, L. R. Krishna, G. Sivakumar, D. S. Rao, G. Padmanabham, *Transactions of the Indian Institute of Metals* **73** (2020) 2141-2159. https://doi.org/10.1007/s12666-020-02053-0

[2] H.-R. Jiang, M.-L. Li, X.-S. Wei, T.-C. Ma, Y. Dong, C.-X. Ying, Z.-Y. Liao, J. Shen, *Journal of Thermal Spray Technology* **28** (2019) 1146-1159. https://doi.org/10.1007/s11666-019-00889-7

[3] X. Gao, C. Li, Y. Xu, X. Chen, X. Han, *Journal of Thermal Spray Technology* **30** (2021) 1875-1890. https://doi.org/10.1007/s11666-021-01250-7

[4] A. R. Govande, A. Chandak, B. R. Sunil, R. Dumpala, *International Journal of Refractory Metals and Hard Materials* **103** (2022) 105776. https://doi.org/10.1016/j.ijrmhm.2021.105772

[5] A. K. Gujba, M. S. Mahdipoor, M. Medraj, *Wear* **484-485** (2021) 203904. https://doi.org/10.1016/j.wear.2021.203904

[6] K. Torkashvand, S. Joshi, V. Testa, F. Ghisoni, S. Morelli, G. Bolelli, L. Lusvarghi, F. Marra, M. Gupta, *Surface and Coatings Technology* **436** (2022) 128296. https://doi.org/10.1016/j.surfcoat.2022.128296

[7] H. L. Alwan, A. V. Makarov, N. N. Soboleva, Y. S. Korobov, V. I. Shumyakov, N. V. Lezhnin, V.A. Zavalishin, *Russian Journal of Non-Ferrous Metals* **62** (2022) 778-784. https://doi.org/10.3103/s1067821221060031

[8] D. C. Ribu, R. Rajesh, D. Thirumalaikumarasamy, S. Vignesh, *Materials Today: Proceedings* **46** (2021) 7518-7530. https://doi.org/10.1016/j.matpr.2021.01.307

[9] Y. Korobov, H. Alwan, N. Soboleva, A. Makarov, N. Lezhnin, V. Shumyakov, M. Antonov, M. Deviatiarov, *Journal of Thermal Spray Technology* **31** (2021) 234-246. https://doi.org/10.1007/s11666-021-01242-7

[10] T. Varis, T. Suhonen, J. Laakso, M. Jokipii, P. Vuoristo, *Journal of Thermal Spray Technology* **29** (2020) 1365-1381. https://doi.org/10.1007/s11666-020-01037-2

[11] E. Avcu, S. Fidan, M.Ö. Bora, O. Çoban, İ. Taşkiran, T. Sinmazçelik, *Advances in Polymer Technology* **32** (2013) E386-E398. https://doi.org/10.1002/adv.21286

[12] S. Fidan, E. Avcu, E. Karakulak, R. Yamanoglu, M. Zeren, T. Sinmazcelik, *Materials Science and Technology* **29** (2013) 1088-1094. https://doi.org/10.1179/1743284713y.0000000239

[13] E. Avcu, Y. Yıldıran Avcu, F. E. Baştan, M. A. U. Rehman, F. Üstel, A. R. Boccaccini, *Progress in Organic Coatings* **123** (2018) 362-373. https://doi.org/10.1016/j.porgcoat.2018.07.021

[14] M. Armağan, A. A. Arici, *Materials and Manufacturing Processes* **32** (2016) 1715-1722. https://doi.org/10.1080/10426914.2016.1269919

[15] D. Mills, *Erosive Wear*, in *Pneumatic Conveying Design Guide*, Elsevier, 2016, pp. 617-642. https://doi.org/10.1016/b978-0-08-100649-8.00027-5.
[16] E. Avcu, S. Fidan, Y. Yıldıran, T. Sınmazçelik, *Tribology - Materials, Surfaces & Interfaces* **7** (2013) 201-210. https://doi.org/10.1179/1751584x13y.0000000043
[17] V. Javaheri, D. Porter, V.-T. Kuokkala, *Wear* **408-409** (2018) 248-273. https://doi.org/10.1016/j.wear.2018.05.010
[18] R. K. Kumar, M. Kamaraj, S. Seetharamu, T. Pramod, P. Sampathkumaran, *Journal of Thermal Spray Technology* **25** (2016) 1217-1230. https://doi.org/10.1007/s11666-016-0427-3
[19] Y. Li, Y. Lian, J. Cao, L. Li, *Proceedings of the Institution of Mechanical Engineers, Part J: Journal of Engineering Tribology* **230** (2015) 634-643. https://doi.org/10.1177/1350650115608209
[20] A. Kumar, A. Sharma, S. K. Goel, *Materials Science and Engineering A* **637** (2015) 56-62. https://doi.org/10.1016/j.msea.2015.04.031
[21] M. S. Mahdipoor, F. Tarasi, C. Moreau, A. Dolatabadi, M. Medraj, *Wear* **330-331** (2015) 338-347. https://doi.org/10.1016/j.wear.2015.02.034
[22] S. Matthews, B. James, M. Hyland, *Surface and Coatings Technology* **203** (2009) 1086-1093. https://doi.org/10.1016/j.surfcoat.2008.10.005
[23] E. Sadeghi, S. Joshi, *Surface and Coatings Technology* **371** (2019) 20-35. https://doi.org/10.1016/j.surfcoat.2019.01.080
[24] L. Baiamonte, S. Björklund, A. Mulone, U. Klement, S. Joshi, *Surface and Coatings Technology* **406** (2021) 126725. https://doi.org/10.1016/j.surfcoat.2020.126725
[25] Y. Lian, Y. Li, *Tribology Online* **13** (2018) 36-42. https://doi.org/10.2474/trol.13.36
[26] A. Hamilton, A. Sharma, U. Pandel, *Surface Review and Letters* **24** (2017) 18500117. https://doi.org/10.1142/s0218625x18500117
[27] S. L. Liu, X. P. Zheng, G. Q. Geng, *Wear* **269** (2010) 362-367. https://doi.org/10.1016/j.wear.2010.04.019
[28] Q. Wang, Z. Tang, L. Cha, *Journal of Materials Engineering and Performance* **24** (2015) 2435-2443. https://doi.org/10.1007/s11665-015-1496-z
[29] J. Liu, L.P. Pan, J. C. Yu, *Materials Science Forum* **686** (2011) 618-622. https://doi.org/10.4028/www.scientific.net/MSF.686.618
[30] Y. Wang, Z. Z. Xing, Q. Luo, A. Rahman, J. Jiao, S. J. Qu, Y. G. Zheng, J. Shen, *Corrosion Science* **98** (2015) 339-353. https://doi.org/10.1016/j.corsci.2015.05.044
[31] R. K. Kumar, M. Kamaraj, S. Seetharamu, S. Anand Kumar, *Materials & Design* **132** (2017) 79-95. https://doi.org/10.1016/j.matdes.2017.06.046
[32] V. Matikainen, S. R. Peregrine, N. Ojala, H. Koivuluoto, J. Schubert, S. Houdkova, P. Vuoristo, *Tribologia - Finnish Journal of Tribology* **36(1-2)** (2019) 58-61. https://doi.org/10.30678/fjt.83590
[33] V. Matikainen, S. Rubio Peregrina, N. Ojala, H. Koivuluoto, J. Schubert, Š. Houdková, P. Vuoristo, *Surface and Coatings Technology* **370** (2019) 196-212. https://doi.org/10.1016/j.surfcoat.2019.04.067
[34] V. Matikainen, H. Koivuluoto, P. Vuoristo, J. Schubert, Š. Houdková, *Journal of Thermal Spray Technology* **27** (2018) 680-694. https://doi.org/10.1007/s11666-018-0717-z
[35] L. L. Silveira, A. G. M. Pukasiewicz, D. J. M. de Aguiar, A. J. Zara, S. Björklund, *Surface and Coatings Technology* **374** (2019) 910-922. https://doi.org/10.1016/j.surfcoat.2019.06.076
[36] V. Matikainen, H. Koivuluoto, P. Vuoristo, *Wear* **446-447** (2020) 203188. https://doi.org/10.1016/j.wear.2020.203188

[37] H. L. Alwan, Y. S. Korobov, N. N. Soboleva, N. V. Lezhnin, A. V. Makarov, M. S. Deviatiarov, *Solid State Phenomena* **299** (2020) 893-901. https://doi.org/10.4028/www.scientific.net/SSP.299.893